Gauge angle dependence in time-dependent Hartree-Fock-Bogoliubov calculations of ^{20}O + ^{20}O head-on collisions with the Gogny interaction

Yukio Hashimoto*
Center for Computational Sciences, University of Tsukuba, Tsukuba 305-8571, Japan

Guillaume Scamps†
Department of Physics, Tohoku University, Sendai 980-8578, Japan
(Received 22 April 2016; published 18 July 2016)

A numerical method to solve time-dependent Hartree-Fock-Bogoliubov equations by using a hybrid basis of two-dimensional harmonic oscillator eigenfunctions and a one-dimensional Lagrange mesh with the Gogny effective interaction is applied to head-on collisions of superfluid ^{20}O nuclei. Taking the energies around the barrier top, the trajectories, pairing energies, and numbers of transferred nucleons are displayed. Their dependence on the relative gauge angle at the initial time is studied.

DOI: 10.1103/PhysRevC.94.014610

I. INTRODUCTION

Nuclear superfluidity has attracted continuous attention among nuclear physicists for more than fifty years. The structure of the nuclear ground states, the reaction mechanism of a pair of colliding nuclei, the dynamical properties of the fission processes, and so on, have been studied in connection with the pairing correlations among the nucleons in the nucleus (nuclei) [1–5].

Time-dependent mean-field theory has been one of the useful theoretical frameworks to study static as well as dynamical properties of nuclei. The time-dependent Hartree-Fock (TDHF) method is the foremost example of the time-dependent mean-field methods. The TDHF method has been widely in use in the investigations of small-amplitude collective vibrations around the ground states as well as large-amplitude collective motions in nuclear fusion/fission processes [6–15]. To deal with the effects of the pairing correlation, TDHF has been extended into the time-dependent Hartree-Fock-Bogoliubov (TDHFB) and TDHF+BCS methods [16–22].

In relation to the reaction processes of two superfluid nuclei, one of the long-standing, interesting subjects is to make clear the mechanism of the particle transfer phenomena influenced by the pairing correlation in the sub-barrier energy region. The particle transfer process between the two superfluid nuclei may be analogous to the *Josephson effect* in solid state physics [23,24]. In the Josephson effect, the electric current flows between two superconducting objects separated by a thin insulator in proportion to the sine of the difference of the phases of the superconducting objects.

In the mean-field framework of the BCS approximation or Hartree-Fock Bogoliubov (HFB) method, the ground state of the superfluid nucleus is accompanied by a time-dependent phase (gauge angle) whose angular velocity is the chemical potential. The phase has no effects on the ground state property of the nucleus, or on its evolution with the TDHFB equations of motion. In the collision process of two superfluid nuclei, the phase of the one nucleus could be different from that of the other. In order to make clear the mechanism of the nuclear Josephson effect [25–30], we propose to study the effects of the difference of the phases (relative phase) between the two initial nuclei.

Recently, several groups have calculated the numbers of transferred nucleons in nuclear collisions by making use of the quantum mechanical method of number projection, in which the angular variables are used as the generator coordinates (integration variables) [22,31–33]. In the framework of the mean-field calculations of the TDHFB method, additional effects of the relative phase are expected on physical quantities such as trajectories, pairing energies, potential profiles, and so on, in the collision processes.

In this article, we propose a numerical technique of solving the TDHFB equations by using the hybrid basis of two-dimensional harmonic oscillator eigenfunctions and a one-dimensional Lagrange mesh [21]. Then, we report its first application to the head-on collision processes of superfluid oxygen ^{20}O nuclei. We study the effects of the relative gauge angle of two colliding nuclei by adopting four different angles (0, 45, 90, and 135 degrees) as representative samples. The dependence of the potentials between the colliding nuclei, trajectories, and pairing energies on the relative phase are discussed.

This article is composed of the following sections: In Sec. II, the TDHFB equations are given together with the initial conditions of the two colliding superfluid nuclei. In Sec. III, the TDHFB calculations of the collision processes of the two oxygen ^{20}O nuclei are carried out with three values of the boost energy, $E_{\rm boost} = 4.8$, 5.0, and 5.2 MeV, leading to center-of-mass energies $E_{\rm c.m.} = 9.21$, 9.41, and 9.61 MeV, respectively. The trajectories, pairing energies, and the number of transferred nucleons are displayed. In Sec. IV, the effects of the initial relative phase (gauge angle) are discussed. Section V is for the summary and concluding remarks.

*hashimoto.yukio.gb@u.tsukuba.ac.jp
†scamps@nucl.phys.tohoku.ac.jp

II. BASIC EQUATIONS AND INITIAL CONDITIONS

A. Basic equation

The nuclear Hamiltonian under consideration is in the form

$$H = \sum_{\alpha\beta} T_{\alpha\beta} C_\alpha^\dagger C_\beta + \frac{1}{4} \sum_{\alpha\beta\gamma\delta} \mathcal{V}_{\alpha\beta\gamma\delta} C_\alpha^\dagger C_\beta^\dagger C_\delta C_\gamma, \tag{1}$$

where $T_{\alpha\beta}$ is the kinetic energy matrix element and $\mathcal{V}_{\alpha\beta\gamma\delta}$ is the antisymmetrized two-body matrix element of the Gogny interaction. The operator $C_\alpha^\dagger$ (C_α) is a nucleon creation (annihilation) operator of a state labeled α.

The quasiparticles $\beta_k^{(\tau)\dagger}$ and $\beta_k^{(\tau)}$ are introduced by the Bogoliubov transformation from the particle operators $C_\alpha^\dagger$ and C_α,

$$\beta_k^{(\tau)\dagger} = \sum_\alpha \left(U_{\alpha k}^{(\tau)} C_\alpha^\dagger + V_{\alpha k}^{(\tau)} C_\alpha \right), \tag{2}$$

$$\beta_k^{(\tau)} = \sum_\alpha \left(U_{\alpha k}^{(\tau)*} C_\alpha + V_{\alpha k}^{(\tau)*} C_\alpha^\dagger \right), \tag{3}$$

where $\tau = p$ (n) for protons (neutrons).

In the TDHFB method, the equations of motion for the matrices $U^{(\tau)}$ and $V^{(\tau)}$ in the Bogoliubov transformation (2) and (3) are given in the form [16,20],

$$i\hbar \frac{\partial}{\partial t} \begin{pmatrix} U^{(\tau)}(t) \\ V^{(\tau)}(t) \end{pmatrix} = \mathcal{H}^{(\tau)} \begin{pmatrix} U^{(\tau)}(t) \\ V^{(\tau)}(t) \end{pmatrix}, \tag{4}$$

with the HFB Hamiltonian $\mathcal{H}^{(\tau)}$,

$$\mathcal{H}^{(\tau)} = \begin{pmatrix} h^{(\tau)} & \Delta^{(\tau)} \\ -\Delta^{(\tau)*} & -h^{(\tau)*} \end{pmatrix}. \tag{5}$$

The mean field Hamiltonian $h^{(\tau)}$ and the pairing mean field $\Delta^{(\tau)}$ are introduced through the relations [2],

$$h_{\alpha\beta}^{(\tau)} = T_{\alpha\beta} + \Gamma_{\alpha\beta}^{(\tau)}, \tag{6}$$

$$\Gamma_{\alpha\beta}^{(\tau)} = \sum_{\gamma\delta} \mathcal{V}_{\alpha\gamma\beta\delta} \rho_{\delta\gamma}^{(\tau)}, \quad \Delta_{\alpha\beta}^{(\tau)} = \frac{1}{2} \sum \mathcal{V}_{\alpha\beta\gamma\delta} \kappa_{\gamma\delta}^{(\tau)}, \tag{7}$$

where $\rho^{(\tau)}$ and $\kappa^{(\tau)}$ are the normal density matrix and pairing tensor,

$$\rho_{\alpha\beta}^{(\tau)} = \left(V^{(\tau)*} V^{(\tau)T} \right)_{\alpha\beta}, \quad \kappa_{\alpha\beta}^{(\tau)} = \left(V^{(\tau)*} U^{(\tau)T} \right)_{\alpha\beta}, \tag{8}$$

respectively. The symbol T in Eq. (8) stands for the transpose of a matrix.

The basis functions labeled α,β, etc. are composed of one-dimensional spatial grid points, i.e., the Lagrange mesh [34,35], in the direction of the z axis and two-dimensional harmonic oscillator eigenfunctions in the directions of the x and y axes [21].

The HFB matrices $U_{\alpha k}^{(\tau)(0)}$ and $V_{\alpha k}^{(\tau)(0)}$ of the ground state of a nucleus are obtained by solving the HFB equations [2]

$$\begin{pmatrix} h^{(\tau)} - \lambda^{(\tau)} & \Delta^{(\tau)} \\ -\Delta^{(\tau)*} & -h^{(\tau)*} + \lambda^{(\tau)} \end{pmatrix} \begin{pmatrix} U_k^{(\tau)} \\ V_k^{(\tau)} \end{pmatrix} = E_k^{(\tau)} \begin{pmatrix} U_k^{(\tau)} \\ V_k^{(\tau)} \end{pmatrix} \tag{9}$$

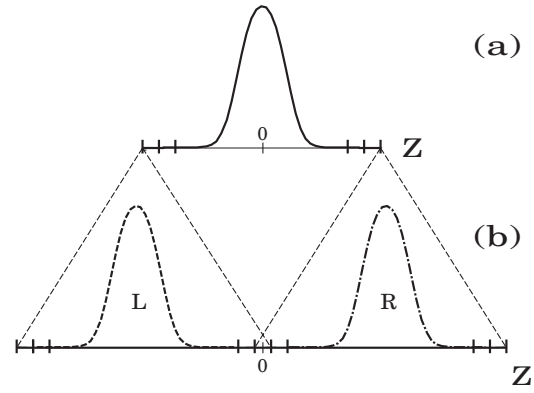

FIG. 1. Initial condition of the TDHFB equation (4). A HFB ground state is calculated by using basis functions with the number of grid points $N_{\rm grid}^{(0)} = N_{\rm grid}/2$ (a). The HFB ground state in (a) is mapped on the space of the basis functions with the number of grid points $N_{\rm grid}$ [L or R in (b)].

with the eigenvalues $E_k^{(\tau)}$ and a chemical potential $\lambda^{(\tau)}$. In Eq. (9), $U_k^{(\tau)}$ ($V_k^{(\tau)}$) denotes the vector $U_{\alpha k}^{(\tau)}$ ($V_{\alpha k}^{(\tau)}$) corresponding to the eigenvalue $E_k^{(\tau)}$ of the quasiparticle with label k.

The inclusion of the chemical potential or any real variable μ in the mean-field Hamiltonians $h^{(\tau)} - \mu$ and $-h^{(\tau)*} + \mu$ in Eq. (5) will keep unchanged the evolution of the one-body density matrix $\rho^{(\tau)}$ and two-body correlation matrix $\kappa^{(\tau)}\kappa^{(\tau)*}$.

B. Initial conditions

When we set up the initial condition of the TDHFB equation (4), we assume that the two nuclei are uncorrelated and independent of each other if the distance between the two nuclei is large enough. With the purpose of realizing the situation, we make use of a Lagrange mesh whose number of the grid points $N_{\rm grid}$ is just double of that of the original Lagrange mesh $N_{\rm grid}^{(0)}$ (Fig. 1): $N_{\rm grid} = 2 \times N_{\rm grid}^{(0)}$.

In the left (L) region with negative z ($z < 0$) in the doubled Lagrange mesh (b) in Fig. 1, the HFB matrices $U_{\alpha k}^{(\tau)(0)}$ and $V_{\alpha k}^{(\tau)(0)}$ of the ground state solution on the Lagrange mesh (a) in Fig. 1 are mapped into the matrices $U_{\alpha k}$ and $V_{\alpha k}$ on the doubled Lagrange mesh,

$$W_{\alpha k}^{(\tau)} = \begin{cases} W_{\alpha k}^{(\tau)(0)}, & \alpha = 1,2,\ldots,N_{\rm base}/2, \\ 0, & \alpha = N_{\rm base}/2+1,\ldots,N_{\rm base}, \end{cases} \tag{10}$$

where $k = 1,2,\ldots,N_{\rm base}/2$ and $W^{(\tau)}$ ($W^{(\tau)(0)}$) stands for the matrix $U^{(\tau)}$ ($U^{(\tau)(0)}$) or $V^{(\tau)}$ ($V^{(\tau)(0)}$). Here, $N_{\rm base}$ is the total number of the basis functions of the two-dimensional harmonic oscillator eigenfunctions and Lagrange mesh together with the spin degrees of freedom.

In the same way, in the right (R) region with positive z ($0 < z$) in the doubled Lagrange mesh, we have the mapped matrices $U_{\alpha k}^{(\tau)}$ and $V_{\alpha k}^{(\tau)}$,

$$W_{\alpha k}^{(\tau)} = \begin{cases} 0, & \alpha = 1,2,\ldots,N_{\rm base}/2, \\ W_{\alpha' k}^{(\tau)(0)} \ (\alpha' = \alpha - N_{\rm base}/2), & \alpha = N_{\rm base}/2+1,\ldots,N_{\rm base}, \end{cases} \tag{11}$$

where $k = N_{\rm base}/2+1,\ldots,N_{\rm base}$ and $W^{(\tau)}$ ($W^{(\tau)(0)}$) is used for the matrix $U^{(\tau)}$ ($U^{(\tau)(0)}$) or $V^{(\tau)}$ ($V^{(\tau)(0)}$).

Note that this initialization method conserves the fermion commutation relations [2],

$$U^{(\tau)\dagger}U^{(\tau)} + V^{(\tau)\dagger}V^{(\tau)} = 1, \tag{12}$$

$$U^{(\tau)}U^{(\tau)\dagger} + V^{(\tau)*}V^{(\tau)T} = 1, \tag{13}$$

$$U^{(\tau)T}V^{(\tau)} + V^{(\tau)T}U^{(\tau)} = 0, \tag{14}$$

$$U^{(\tau)}V^{(\tau)\dagger} + V^{(\tau)*}U^{(\tau)T} = 0. \tag{15}$$

Each of the two nuclei is boosted with a momentum so that the total momentum of the system is zero and the initial position of the center of mass is kept at the initial point.

III. HEAD-ON COLLISIONS OF TWO ^{20}O NUCLEI

In the present calculations, the Gogny D1S is used as the effective interaction. We note that the Coulomb force is used only in the mean-field part and is not included in the pairing part of the HFB Hamiltonian.

The parameters used in the calculations are as follows: The grid spacing $\Delta z = 0.91$ fm and the total number of the grid points of the doubled Lagrange mesh $N_{\rm grid}$ is 46. The harmonic oscillator eigenfunctions are used as the basis functions in the x-y plane. The space of the harmonic oscillator quantum number is restricted as $n_x + n_y \leqslant N_{\rm shell} = 4$ with the quantum number n_x (n_y) in the direction of the x (y) axis. The total number of basis functions $N_{\rm base}$ is $N_{\rm base} = (N_{\rm shell}+1)(N_{\rm shell}+2)N_{\rm grid}$ including spin up and spin down. The harmonic oscillator parameter $\hbar\omega = 14.6$ MeV and the maximum number $N_{\rm shell}$ are used in the calculations of the HFB ground state solutions (a) in Fig. 1 as well as the head-on collisions of the two nuclei on the doubled mesh space (b) in Fig. 1.

Here, we note that the restricted space limits the number of degrees of freedom to 2760 including spin and isospin, while a full calculation in Cartesian mesh would involve around 10^5 degrees of freedom. The CPU time for one step of the integration of the TDHFB equations is four minutes on a Hitachi SR16000M1 using 512 CPUs. It takes 8 to 10 days to calculate a single trajectory in the subsequent sections.

A. Relative distance, relative momentum, and number of transferred particles

The evolution of the system is shown in Fig. 2 for the center-of-mass energies $E_{\rm c.m.}$, where one is below the barrier and another is above the barrier. For the energy $E_{\rm c.m.}$ below the barrier, the two nuclei exchange nucleons and separate into two fragments, while the two nuclei merge into one for the energy $E_{\rm c.m.}$ above the barrier.

In order to understand the dynamical properties of the collision processes around the barrier, we followed Washiyama's method of introducing a section plane at a point on the z axis between the two colliding nuclei [12]. The section plane is set at the point $z = z_{\rm s}$ where the density $\tilde{\rho}_{\rm L}(\mathbf{r},t)$ is equal to the density $\tilde{\rho}_{\rm R}(\mathbf{r},t)$. Here, $\tilde{\rho}_{\rm L/R}(\mathbf{r},t)$ is the density that is made from the vectors $V^{(\tau)}_{\alpha k}$ which started from the nucleus in the left

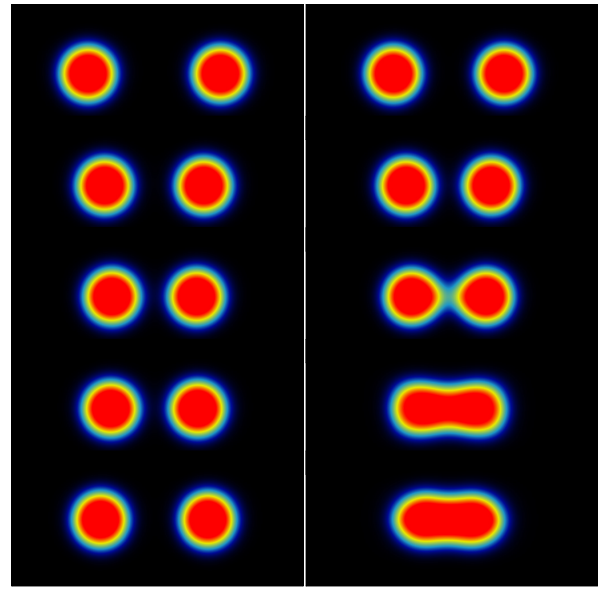

FIG. 2. Densities in the y-z plane in the collisions ^{20}O+^{20}O for the center-of-mass energies $E_{\rm c.m.} = 9.21$ MeV (left) and $E_{\rm c.m.} = 9.61$ MeV (right). The densities are shown with respect to the time at times $ct = 180$, 360, 540, 720, and 900 fm from top to bottom, respectively. c is light speed.

(L) [right (R)] region at the initial time $t = 0$,

$$\tilde{\rho}_{\rm L/R}(\mathbf{r},t) = \sum_{\alpha\beta}\Phi_\alpha(\mathbf{r})\Phi^*_\beta(\mathbf{r})\tilde{\rho}^{\rm L/R}_{\alpha\beta}\delta_{\sigma_\alpha\sigma_\beta}, \tag{16}$$

with the density matrix $\tilde{\rho}^{\rm L/R}_{\alpha\beta}$,

$$\tilde{\rho}^{\rm L/R}_{\alpha\beta} = \sum_{\tau=p,n}\sum_{k'}V^{(\tau)*}_{\alpha k'}V^{(\tau)}_{\beta k'}. \tag{17}$$

The index k' takes the values $k' = 1,2,\ldots,N_{\rm base}/2$ for $\tilde{\rho}^{\rm L}_{\alpha\beta}$ and $k' = N_{\rm base}/2+1, N_{\rm base}/2+2,\ldots,N_{\rm base}$ for $\tilde{\rho}^{\rm R}_{\alpha\beta}$. In (16), $\Phi_\alpha(\mathbf{r})$ and $\Phi_\beta(\mathbf{r})$ are the basis functions of the two-dimensional harmonic oscillator eigenfunctions and Lagrange mesh [21], and σ_α etc. are the labels of the spin.

Making use of the section plane at $z = z_{\rm s}$, we calculated the number of the nucleons in the left and right regions with respect to the plane,

$$m_{\rm L} = \int d^3x\ \rho(\mathbf{r})\theta(z_{\rm s}-z), \tag{18}$$

$$m_{\rm R} = \int d^3x\ \rho(\mathbf{r})\theta(z-z_{\rm s}), \tag{19}$$

with the total density $\rho(\mathbf{r}) = \rho^{(p)}(\mathbf{r}) + \rho^{(n)}(\mathbf{r})$ from the proton (p) and neutron (n) densities.

The center-of-mass position $z_{\rm L}$ ($z_{\rm R}$) and momentum $p_{\rm L}$ ($p_{\rm R}$) in the left (right) region divided by the section plane are calculated,

$$z_{\rm L} = {\rm Tr}[(z)^{\rm (L)}\rho]/m_{\rm L}, \quad z_{\rm R} = {\rm Tr}[(z)^{\rm (R)}\rho]/m_{\rm R} \tag{20}$$

and

$$p_{\rm L} = {\rm Tr}[(p_z)^{\rm (L)}\rho], \quad p_{\rm R} = {\rm Tr}[(p_z)^{\rm (R)}\rho], \tag{21}$$

respectively. In Eqs. (20) and (21), the notation Tr is the trace of a matrix, and the notations $(z)^{(\mathrm{L})}$, $(z)^{(\mathrm{R})}$, $(p_z)^{(\mathrm{L})}$, and $(p_z)^{(\mathrm{R})}$ stand for matrices with the matrix elements

$$(z)^{(\mathrm{L})}_{\alpha\beta} = \int d^3x\, \theta(z_\mathrm{s} - z)\Phi_\alpha(\mathbf{r})^* z \Phi_\beta(\mathbf{r})\delta_{\sigma_\alpha\sigma_\beta},$$
$$(p_z)^{(\mathrm{L})}_{\alpha\beta} = \int d^3x\, \theta(z_\mathrm{s} - z)\Phi_\alpha(\mathbf{r})^* \left(-i\hbar\frac{\partial}{\partial z}\right)\Phi_\beta(\mathbf{r})\delta_{\sigma_\alpha\sigma_\beta}, \tag{22}$$

$$(z)^{(\mathrm{R})}_{\alpha\beta} = \int d^3x\, \theta(z - z_\mathrm{s})\Phi_\alpha(\mathbf{r})^* z \Phi_\beta(\mathbf{r})\delta_{\sigma_\alpha\sigma_\beta},$$
$$(p_z)^{(\mathrm{R})}_{\alpha\beta} = \int d^3x\, \theta(z - z_\mathrm{s})\Phi_\alpha(\mathbf{r})^* \left(-i\hbar\frac{\partial}{\partial z}\right)\Phi_\beta(\mathbf{r})\delta_{\sigma_\alpha\sigma_\beta}. \tag{23}$$

Here, ρ is the total density matrix $\rho = \rho^{(p)} + \rho^{(n)}$. The relative coordinate R and relative momentum P_z are defined as

$$R = z_\mathrm{R} - z_\mathrm{L},$$
$$P_z = (m_\mathrm{L} p_\mathrm{R} - m_\mathrm{R} p_\mathrm{L})/(m_\mathrm{L} + m_\mathrm{R}). \tag{24}$$

B. Trajectories, pairing energies, and number of transferred particles

As examples of the head-on collisions of two ^{20}O nuclei, we chose three boost energies $E_\mathrm{boost} = 4.8$, 5.0, and 5.2 MeV, leading to the center-of-mass energies $E_\mathrm{c.m.} = 9.21$, 9.41, and 9.61 MeV, respectively.

In Fig. 3, we display the frozen density potential $V_\mathrm{FD}(R)$ with respect to the relative distance R together with the positions of the three initial energies to show that they are below, nearly on, and above the top of the frozen density potential, respectively.

Corresponding to the three energies $E_\mathrm{c.m.}$, we got three trajectories of the colliding oxygen ^{20}O nuclei in the phase space $R - P_z$ of the relative distance R and the relative momentum P_z.

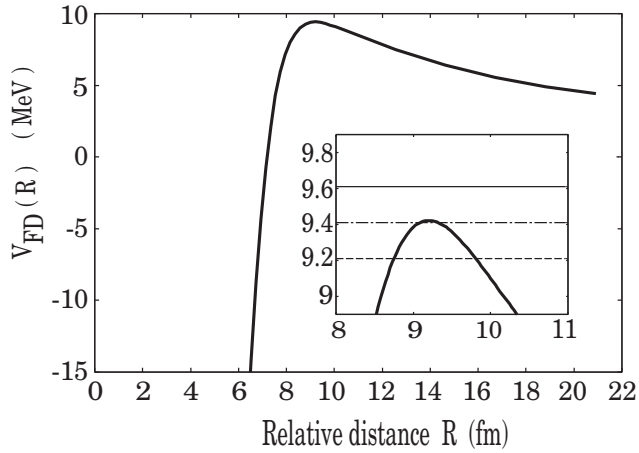

FIG. 3. The frozen density potential $V_\mathrm{FD}(R)$ with respect to relative coordinate R of the head-on collision of two ^{20}O nuclei. The inset is the magnification of the region around the top of the frozen density potential. In the inset, three energies are described with dashed, dash-dotted, and solid lines for $E_\mathrm{c.m.} = 9.21$, 9.41, and 9.61 MeV, respectively.

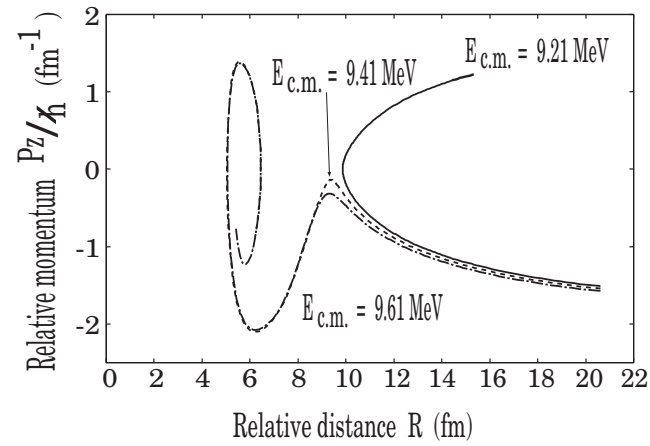

FIG. 4. Trajectories in the phase space of the relative coordinate R and the relative momentum P_z. The solid (dashed, dash-dotted) curve corresponds to the initial energy $E_\mathrm{c.m.} = 9.21$ (9.41, 9.61) MeV. The two trajectories with $E_\mathrm{c.m.} = 9.41$ and 9.61 MeV almost fully overlap in the region $R < 8.5$ fm.

In Fig. 4, we display the three trajectories in the phase space $R - P_z$. They start at $R = 20.91$ fm and follow each other side by side till they come to around $R \sim 12$ fm. After passing a point around $R \sim 12$ fm, the three trajectories begin to separate from each other: The trajectory with energy $E_\mathrm{c.m.} = 9.21$ MeV corresponds to a process in which the two oxygen ^{20}O nuclei come near each other, stop at the turning point around $R \sim 10$ fm, and then bounce back into two fragments. The two fragments are mixtures of the components such as the transferred states and the two ^{20}O nuclei in their ground and excited states.

The two trajectories with energies $E_\mathrm{c.m.} = 9.41$ and 9.61 MeV, on the other hand, represent the process of fusion of the two nuclei after slowing down in relative motion. The combined systems display vibration after the fusion of the two ^{20}O's in both cases of these energies.

In Fig. 5, the variations of the pairing energies along the three trajectories in Fig. 4 are displayed. We see that the pairing energies are kept almost constant before the two nuclei come to the region of the top of the potential energy $V_\mathrm{FD}(R)$ at around $R \sim 9.2$ fm for the cases of the energies $E_\mathrm{c.m.} = 9.41$ and 9.61 MeV. In a similar way, the pairing energy is kept almost constant until the two nuclei come to the turning point at around $R \sim 10.0$ fm for the case with energy $E_\mathrm{c.m.} = 9.21$ MeV.

Once the two nuclei begin to fuse in the cases of energies $E_\mathrm{c.m.} = 9.41$ and 9.61 MeV, the pairing energy E_pair rapidly becomes small in magnitude, from -13 to -2 MeV, and oscillates around the value $E_\mathrm{pair} \sim -2$ MeV in each case of the energies (a) and (b) in Fig. 5. We can interpret this diminution of the pairing energy as due to the increase of the excitation energy after fusion. The occurrence of internal excitations is expected to reduce the pairing correlation. When the two nuclei turn back from the turning point (c) in Fig. 5, on the other hand, the variation of the pairing energy is 0.15 MeV.

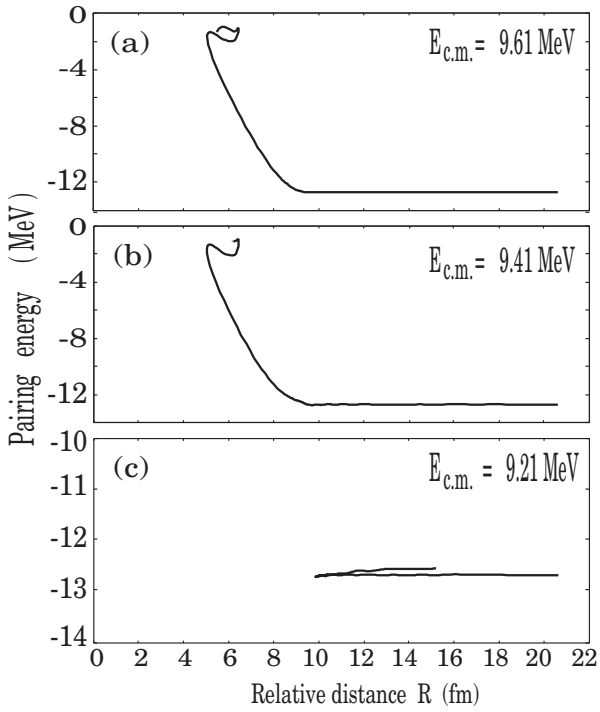

FIG. 5. Pairing energies of the trajectories with the energies $E_{\text{c.m.}} = 9.61$ MeV (a), 9.41 MeV (b), and 9.21 MeV (c) are plotted with respect to the relative distance R.

In relation to the variations of the pairing energies in Fig. 5, let us calculate the numbers of transferred nucleons. We followedWashiyama's definition of the number of transferred nucleons $N^{\text{L/R}}_{\text{trans}}[R(t)]$ in the collision process of a pair of the identical nuclei, which was used in the framework of the TDHF method [12];

$$N^{\text{L}}_{\text{trans}}[R(t)] = \int d^3x \tilde{\rho}_{\text{L}}(\mathbf{r},t)\theta(z), \tag{25}$$

where L stands for the left nuclei at the initial time $t = 0$ and the density $\tilde{\rho}_{\text{L/R}}(\mathbf{r},t)$ is given in (17). We paid attention only to the transfer of nucleons which were in the left nuclei at the initial time, since the present system of two oxygen ^{20}O nuclei is symmetric with respect to the origin $z = 0$. Then, the section plane is also put at the origin $z_s = 0$.

In Figs. 6 and 7, we show numbers of transferred protons and neutrons with respect to the relative distance R in the cases of trajectories with energies $E_{\text{c.m.}} = 9.61$ and 9.21 MeV, respectively.

In Fig. 6, the two nuclei are in the process of fusion within the region $R \leqslant 9.2$ fm, and the numbers of transferred protons and neutrons rapidly increase as the overlap of the two nuclei becomes larger. In the figure, multiplying the number of transferred protons by 1.5, we get a curve which goes along the curve of the number of transferred neutrons. Since the value 1.5 is just the value of the N/Z ratio in ^{20}O, we see that the protons and neutrons begin to move into the region of the other nuclei in a similar way after the combined system passes over the top of the potential energy $V_{\text{FD}}(R)$.

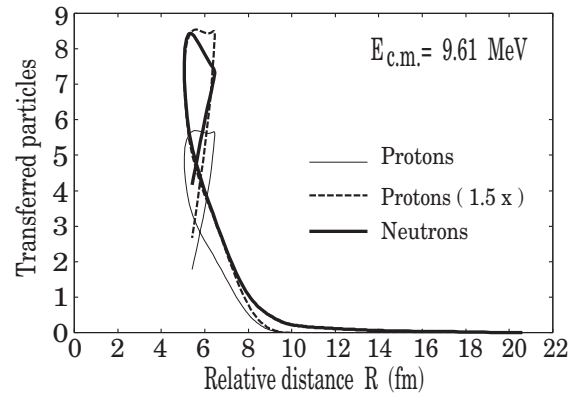

FIG. 6. Numbers of transferred protons (thin curve) and neutrons (thick curve) with respect to the relative distance along the trajectory with energy $E_{\text{c.m.}} = 9.61$ MeV. The broken curve is plotted by multiplying the number of transferred protons by a factor of 1.5.

In the region $R \geqslant 9.2$ fm, the number of transferred protons is practically zero, while the number of transferred neutrons slowly increases to a value of around 0.4 as the two nuclei approach each other.

In Fig. 7, the energy of the system is below the top energy of the potential curve $V_{\text{FD}}(R)$. The numbers of transferred nucleons are small along the trajectory in which the system's nuclei approach each other, stop at the turning point, and separate again into two fragments.

The number of transferred protons increase only when the system is near the turning point, though it is much smaller than that of the neutrons under the influence of the Coulomb potential.

The number of transferred neutrons increases monotonically up to 0.2 as the two nuclei approach each other before they come to the turning point $R \sim 10.0$ fm. The number of transferred neutrons jumps up by 0.2 near the turning point, and comes up to 0.55 at the end point of the curve in Fig. 7 at the distance $R \sim 18$ fm. As a result, the number of transferred

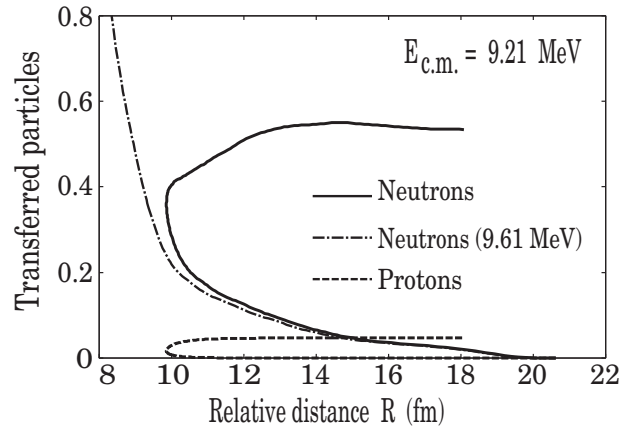

FIG. 7. Numbers of transferred protons (broken curve) and neutrons (solid curve) with respect to the relative distance in the trajectory with energy $E_{\text{c.m.}} = 9.21$ MeV. The dash-dotted curve is for the number of transferred neutrons in Fig. 6 as a reference.

neutrons is more than ten times as large as that of the protons in the whole process in Fig. 7. The ratio is much larger than the N/Z ratio 1.5 in ^{20}O. The Coulomb barrier is the main reason for the difference between the numbers of transferred protons and neutrons.

In Fig. 7, we also note that the transferred-neutron curve for the trajectory with energy $E_{\rm c.m.} = 9.21$ MeV follows that of the trajectory with energy $E_{\rm c.m.} = 9.61$ MeV in Fig. 6 in the approach stage of the two nuclei, before they come to the region near the turning point. This could be understood from the variations of the pairing energies in Fig. 5: We see that the pairing energies of the trajectories for the three energy cases are kept practically constant at the initial values during the two nuclei's approach to each other. The tail parts of the neutron densities of the approaching ^{20}O nuclei with the same pairing energies are almost the same. Then, the numbers of transferred neutrons during the approach stage of the two nuclei could have a common tendency among the three energy cases.

IV. EFFECTS OF THE INITIAL RELATIVE GAUGE ANGLE

In the superfluid nuclei which satisfy the HFB equations (9), it is well known that there is a gauge invariance in relation to the transformation in terms of an operator $G(\chi) = e^{-i\chi\hat{N}}$, with the number operator $\hat{N}$. The operator $G(\chi)$ transforms the matrices $U_{\alpha k}$ and $V_{\alpha k}$ to $e^{-i\chi}U_{\alpha k}$ and $e^{i\chi}V_{\alpha k}$, respectively. The transformation does not change the properties of the nucleus in the ground state as long as an isolated nucleus is under consideration. In the collision process of two superfluid nuclei, however, we do not know in advance the effects of the gauge transformations in the two nuclei at the initial time on the properties of the two nuclei colliding on the trajectory.

From the quantum mechanical point of view, the degree of of freedom of the transformation by the operator $G(\chi)$ is used to project out a state with a specified number of particles from the HFB state.

In the framework of the mean field of the (TD)HFB method, what we would like to study is the influence of the gauge transformations within the HFB ground states at the initial stage of the colliding nuclei on the behavior of the system later in the collision process.

A. A combination of ^{16}O and ^{20}O

As an example of the case in which the gauge transformation of the superfluid nucleus plays no effects on the collision process, we take the combination of ^{16}O and ^{20}O. We adopt the phase factors $e^{i\chi}$ with $\chi = 0$, 45, 90, and 135 degrees as the representation of the gauge transformation in the superfluid nucleus ^{20}O,

$$U_{\alpha k} = e^{i\chi}U^{(0)}_{\alpha k}, \quad V_{\alpha k} = e^{-i\chi}V^{(0)}_{\alpha k}. \tag{26}$$

The ^{16}O is not in the superfluid phase but in the normal state for both protons and neutrons. Note that this transformation keeps the normal density unchanged and modifies the pairing tensor κ with a phase shift 2χ. In consequence the values of χ between 180 and 360 degrees are redundant with the values between 0 and 180 degrees.

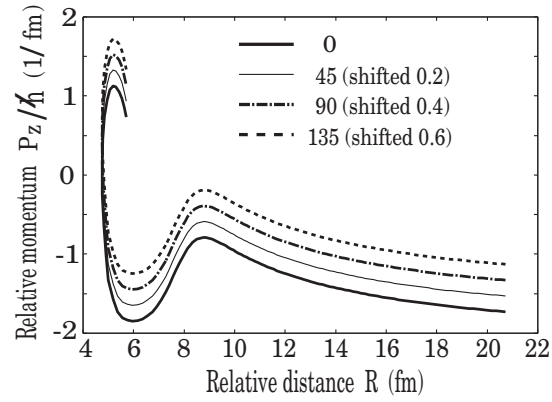

FIG. 8. Trajectories of head-on collisions of ^{16}O and ^{20}O with energy $E_{\rm c.m.} = 11.41$ MeV in the phase space of the relative distance R and relative momentum P_z. The solid (thin solid, dot-dashed, and dashed) curve is for the case with initial gauge angle $\chi = 0$ (45, 90, and 135) degrees. All of the trajectories overlap each other. The curve with $\chi = 45$ (90, 135) degrees is shifted upward by 0.2 (0.4, 0.6) 1/fm for readability.

We put ^{16}O as the left-hand side nucleus and ^{20}O with the phase factors in Eq. (26) as the right-hand side nucleus in the initial conditions (10) and (11). In the case of energy $E_{\rm c.m.} = 11.41$ MeV, the trajectories are shown in Fig. 8, with the different initial gauge angles $\chi = 0$, 45, 90, and 135 degrees. All of the trajectories in Fig. 8 with different initial gauge angles overlap each other completely.

The variations of the pairing energies with respect to the relative distance are shown in Fig. 9 in the cases of the different initial gauge angles χ. After passing the region of the top of the potential energy at $R \sim 8.5$ fm, the pairing energies smoothly decrease to -2 MeV and oscillate about the value. Again, the curves of the pairing energies with different initial gauge angles overlap each other completely.

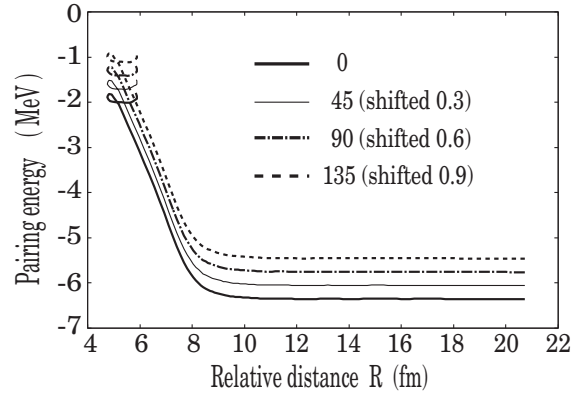

FIG. 9. Variations of the pairing energies with respect to the relative distance in the collision processes in Fig. 8. The solid (thin solid, dot-dahsed, and dashed) curve is for the case with initial gauge angle $\chi = 0$ (45, 90, and 135) degrees. All of the curves overlap each other. The curve with $\chi = 45$ (90, 135) degrees is shifted upward by 0.3 (0.6, 0.9) MeV for readability.

Thus, we see that there is no dependence on the initial gauge angles in the collision process of the combination of a nucleus in the normal state and a superfluid nucleus. This result can be understood simply from the fact that the normal nucleus does not break the gauge angle symmetry. In consequence, changing the phase of the superfluid nuclei is equivalent to changing the whole phase of the system, in which transformation the evolution of the observables is kept unchanged.

B. A combination of ^{20}O and ^{20}O

In the case of the combination of ^{20}O and ^{20}O, we follow the way of setting the initial condition of the TDHFB equations which is stated in the previous subsection for the case of collisions of ^{16}O and ^{20}O. The initial phase factors $e^{i\chi}$ with $\chi = 0$, 45, 90, and 135 degrees are applied in the HFB solutions $U^{(0)}_{\alpha k}$ and $V^{(0)}_{\alpha k}$ of the ground state of ^{20}O just as in (26). Then each of the set of matrices $e^{i\chi}U^{(0)}_{\alpha k}$ and $e^{-i\chi}V^{(0)}_{\alpha k}$ is mapped as the right-hand side nucleus, while the HFB solutions $U^{(0)}_{\alpha k}$ and $V^{(0)}_{\alpha k}$, which is just the case with the gauge angle $\chi = 0$, are mapped as the left-hand side nucleus.

In Figs. 10 and 11, we show the trajectories in the case of energy $E_{\rm c.m.} = 11.41$ MeV. The latter figure, Fig. 11, is a magnification of the region with relative distance $4 \leqslant R \leqslant 11$ fm in the former figure, Fig. 10.

In contrast to the cases of the combination of ^{16}O and ^{20}O in the previous subsection, the trajectories are dependent on their initial gauge angles and are separated from each other in the region of relative distance $R \leqslant 10$ fm. The shift of the trajectory with the initial gauge angle $\chi = 90$ degrees from the one with the angle $\chi = 0$ degree is the largest. The trajectories with angles $\chi = 45$ and 135 degrees overlap each other and come in the space between the trajectories withangles $\chi = 0$ and 90 degrees.

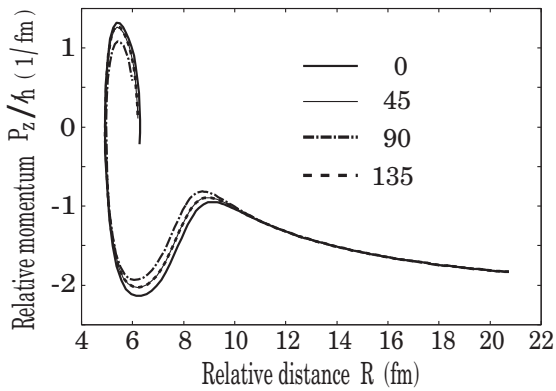

FIG. 10. Trajectories of head-on collisions of ^{20}O and ^{20}O with energy $E_{\rm c.m.} = 11.41$ MeV in the phase space of the relative distance R and relative momentum P_z. Each of the trajectories is the result of the first 2000 steps of the time integration of the TDHFB equations (4). The solid (thin solid, dot-dashed, and dashed) curve is for the case with initial gauge angle $\chi = 0$ (45, 90, and 135) degrees. The trajectories with initial gauge angles $\chi = 45$ and 135 degrees overlap each other.

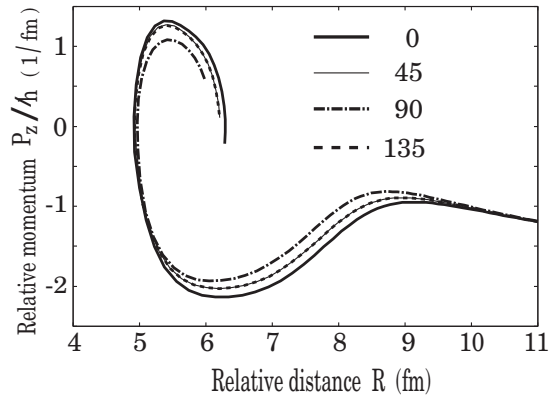

FIG. 11. Magnification of the region of relative distance $R \leqslant 11$ fm in Fig. 10.

Just as in the cases of the trajectories, the variation of the pairing energy with respect to the relative distance R changes as the gauge angle χ is varied. In Fig. 12, we plot the pairing energies of the trajectories in Fig. 11 with respect to the relative distance R for initial gauge angles $\chi = 0$, 45, 90, and 135 degrees. The size of the shift of the pairing energy with gauge angle $\chi = 90$ degrees from that with $\chi = 0$ degrees is the largest among the three cases of gauge angles.

In Figs. 13 and 14, we show the trajectories in the case of energy $E_{\rm c.m.} = 9.21$ MeV. The latter figure, Fig. 14, is a magnification of the region with relative distance $9.8 \leqslant R \leqslant 11$ fm in the former figure, Fig. 13.

Just in the same way as the case with energy $E_{\rm c.m.} = 11.41$ MeV, the trajectories are dependent on the initial gauge angles χ, and the shift of the trajectory with angle $\chi = 90$ degrees from that with angle $\chi = 0$ is the largest. The two trajectories with angles $\chi = 45$ and 90 degrees overlap each other.

A remarkably different point in the trajectories with energies $E_{\rm c.m.} = 11.41$ MeV and $E_{\rm c.m.} = 9.21$ MeV is as follows: In the case of energy $E_{\rm c.m.} = 11.41$ MeV, the point of the relative distance at which the relative momentum P_z takes the smallest absolute value shifts to the direction of the small

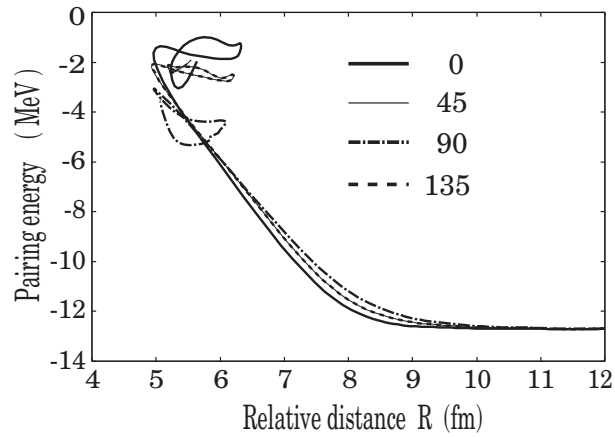

FIG. 12. Variation of the pairing energies with respect to the relative distance R in the trajectories in Fig. 11.

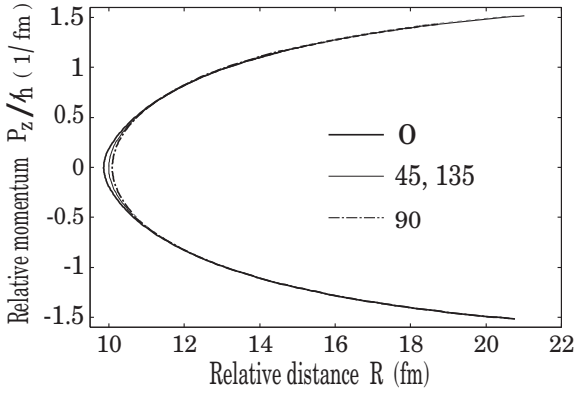

FIG. 13. Trajectories of head-on collisions of ^{20}O and ^{20}O with energy $E_{\rm c.m.} = 9.21$ MeV in the phase space of the relative distance R and relative momentum P_z. The solid (dash-dotted) curve is for the case with initial gauge angle $\chi = 0$ (90) degrees. The thin solid curve is for both $\chi = 45$ and 135 degrees. The trajectories with angles $\chi = 45$ and 135 degrees overlap each other.

value of R, when the initial gauge angle is varied from 0 to 90 degrees through 45 degrees. On the other hand, in the case of energy $E_{\rm c.m.} = 9.21$ MeV, the turning point of the trajectory shifts toward the large value of R when the gauge angle is varied as $\chi = 0$, 45, and 90 degrees.

The difference could be understood from the change of the shapes of the frozen density potential energies with respect to the relative distance R when the gauge angle χ is varied. In Fig. 15, we plot the frozen density potential energy curves near the point $R = 9$ fm with the gauge angles $\chi = 0$, 45, 90, 135 degrees. We see that the top of the energy curve shifts to the direction of the small value of R when the gauge angle is varied as $\chi = 0$, 45, 90 degrees. This is consistent with the shift of the value of R at which the relative momentum P_z takes the minimum absolute value in the case of energy $E_{\rm c.m.} = 11.41$ MeV. Together with the shift of the tops of the frozen density potential energy curves, they are shifted upward when the gauge angle is varied as $\chi = 0$, 45, and 90 degrees.

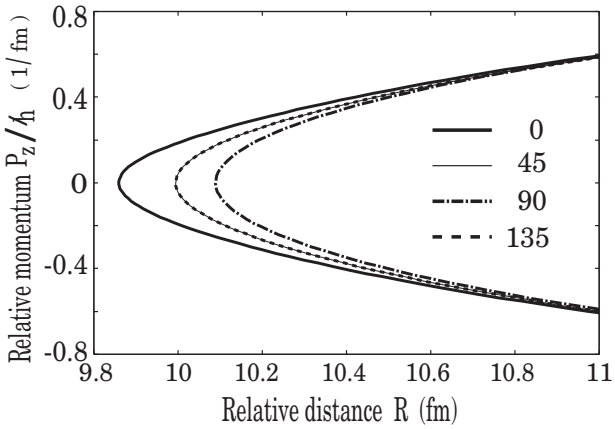

FIG. 14. Magnification of the region of relative distance $9.8 \leqslant R \leqslant 11$ fm in Fig. 13. The solid (thin solid, dashed, and dash-dotted) curve is for the case with gauge angle $\chi = 0$ (45, 90, and 135) degrees.

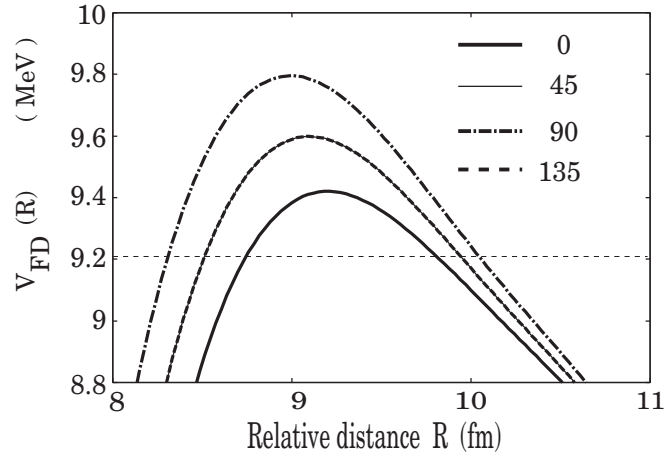

FIG. 15. The frozen density potentials $V_{\rm FD}(R)$ with respect to the relative distance R with the initial gauge angles $\chi = 0$ (solid), 45 (thin solid), 90 (dash-dotted), and 135 (dashed) degrees. The thin dashed line stands for the energy $E_{\rm c.m.} = 9.21$ MeV.

Then, the section of the potential energy curve with energy $E_{\rm c.m.} = 9.21$ MeV shifts toward the large value of R. This is consistent with the shift of the turning points of the trajectories in Fig. 14 with the angles $\chi = 0$, 45, and 90 degrees.

To understand this phenomenon, we can look at the total energy in the frozen calculation that is directly related to the nucleus-nucleus potential in Fig. 15. Because the normal density is not affected by the relative phase, only the pairing part of the total energy changes with the choice of the relative gauge angle,

$$E_{\rm pair} = \frac{1}{4} \sum_{\alpha\beta\gamma\delta} \overline{v}_{\alpha\beta\gamma\delta} \kappa^*_{\alpha\beta} \kappa_{\gamma\delta}. \tag{27}$$

The κ matrix can be decomposed into a part coming from the left nucleus and a part coming from the right. Because the phase of the κ coming from the right part is shifted by 2χ, the total κ matrix is expected to be minimum for the angle $\chi = 90$ degrees. This phase dependence of the potential energy illustrates that the nucleus-nucleus interaction energy for $\chi = 90$ degrees is smaller than that for $\chi = 0$. Here, the nucleus-nucleus interaction energy is the difference between the Coulomb energy and the frozen density potential energy at each point of the relative distance R.

Let us pay attention to the variations of the number of neutrons in the left region. The left and right regions are separated by a section plane located at $z = z_s$ that was introduced in Sec. III.

In Figs. 16 and 17, we show the variations of the numbers of the neutrons with respect to the relative distance R when the gauge angle is varied as $\chi = 0$, 45, 90, and 135 degrees. Each of the curves in the figures stands for the difference of the number $N_{\rm L}$ of the neutrons in the left region from the initial value 12. $N_{\rm L}$ is calculated as in Eq. (18) with $\rho(\mathbf{r})$ replaced by the neutron density $\rho^{(n)}(\mathbf{r})$,

$$N_{\rm L} = \int d^3x\, \rho^{(n)}(\mathbf{r}) \theta(z_{\rm s} - z). \tag{28}$$

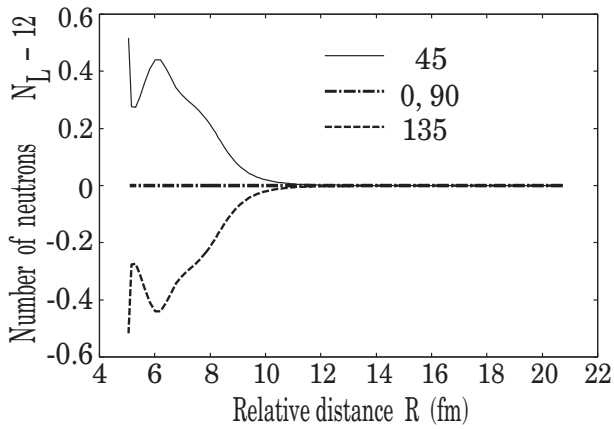

FIG. 16. Variation of the number $N_{\rm L}$ of the neutrons in the left region with respect to the relative distance R for energy $E_{\rm c.m.} =$ 11.41 MeV. The thin solid (dashed) curve is for the case with gauge angle $\chi = 45$ (135) degrees. The dot-dashed curve is for the cases with $\chi = 0$ and 90 degrees. The two curves of the cases with $\chi = 0$ and 90 degrees overlap each other.

In both of the figures, the curves for the gauge angles $\chi = 0$ and 90 degrees are flat, denoting that the numbers of neutrons in the left region are kept at 12 all along the trajectories. In the cases of trajectories with gauge angles $\chi = 45$ and 135 degrees, on the other hand, the number of neutrons increases (decreases) for gauge angle $\chi = 45$ (90) degrees in the left region.

In Fig. 17, we see that the change of the number $N_{\rm L}$ of neutrons is realized near the turning point of the trajectory of the bouncing nuclei. When the number $N_{\rm L}$ of neutrons is plotted with respect to the elapsed time in Fig. 18, the smooth variation of the number $N_{\rm L}$ is clearly illustrated. Thus, Figs. 16 to 18 suggest to us the dependence of the number $N_{\rm L}$ on the relative gauge angle $\Phi = 2\chi$ with periodicity 2π.

Taking account of the one-dimensional situation of the present calculations of head-on collisions, and assuming the 2π periodicity of the number $N_{\rm L}$ of neutrons in the left region with respect to the relative gauge angle Φ, we guess that the

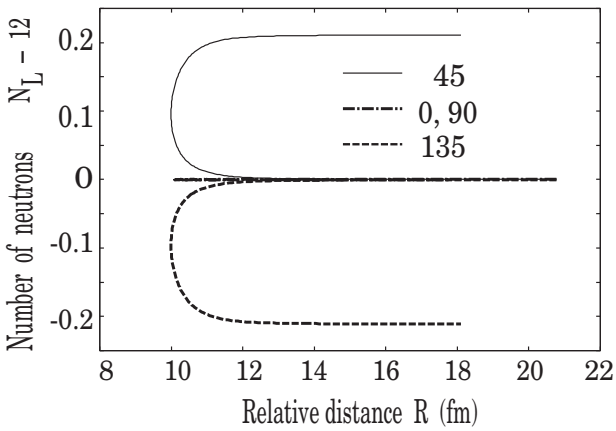

FIG. 17. The same as in Fig. 16, but for the energy $E_{\rm c.m.} =$ 9.21 MeV.

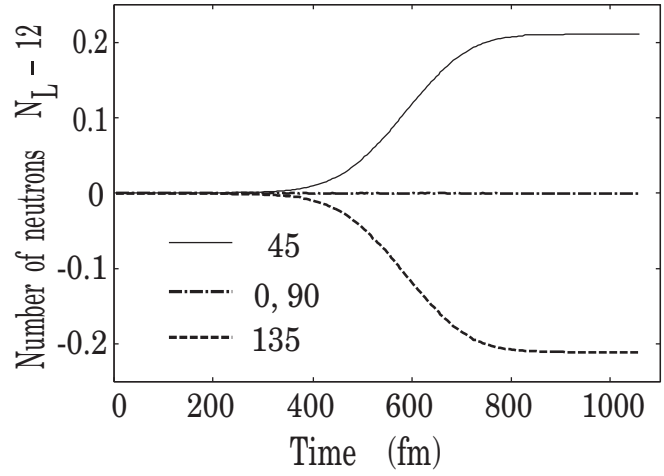

FIG. 18. The same as in Fig. 17, but the variations of the number $N_{\rm L}$ of the neutrons in the left region are plotted with respect to the elapsed time.

flux $J_{\rm s}$ of the neutrons across the section plane at $z = z_{\rm s}$ is proportional to the sine of the angle Φ,

$$J_{\rm s} \propto \sin(\Phi). \tag{29}$$

The relation in (29) reminds us of the Josephson current of an electron pair through a Josephson junction with a relative phase Φ of the two superconducting objects separated by a thin insulator [23,24]. Detailed studies are needed to understand the microscopic background of the flows of nucleons under the condition of superfluidity illustrated in Figs. 16 to 18.

V. SUMMARY AND CONCLUDING REMARKS

In this article, we have reported the first results of the application of a method of solving TDHFB equations with the Gogny force to the head-on collision processes of the superfluid nuclei ^{20}O $+^{20}$O. The method of solving the TDHFB equations is realized by using two-dimensional harmonic oscillator eigenfunctions and a one-dimensional Lagrange mesh [21]. A candidate way of setting up the initial conditions of the collision processes was proposed.

The advantage of the present numerical method is the natural cutoff for quasiparticle energy obtained by using a Gaussian type finite range interaction. Furthermore, the choice of the present hybrid basis allows one to include all the quasiparticle states, so the unitarity relations (12) to (15) are respected during the evolution. These two points are expected to contribute to stable numerical integrations of the TDHFB equations.

Setting the energies of the colliding nuclei around the energy of the top of the frozen density potential energy, we have displayed the trajectories, variations of the pairing energies with respect to the relative distance, and the numbers of transferred nucleons.

We studied the effects of the initial relative phase on the properties of the colliding superfluid nuclei. In particular, the dependence of the trajectories, pairing energies, and number of transferred neutrons on the relative phase was visually

illustrated in the figures. We showed that the static and dynamical nucleus-nucleus potential depends on the relative gauge angle between two superfluid nuclei. For the reaction $^{20}O+^{20}O$ the difference of the potential energy is about 0.4 MeV for the height of the barrier and 0.2 fm for the position of the barrier.

Some remarks concerning the present calculations are as follows:

(1) The setup the initial conditions of the TDHFB equations of the colliding superfluid nuclei was of a *sharp cutoff* type, by assuming that the correlations of the two nuclei at the initial time could be neglected when they were set apart with large distance. At present, the effects of the sharp cutoff initial conditions have not been studied. It would be interesting to compare the results of the present calculations with those obtained by using other types of initial conditions.

(2) In all of the numerical calculations in this article, we have used a fixed set of the parameters of the basis functions (number of the grid points $N_{\rm grid}$, grid size Δz, maximum number of the two-dimensional harmonic oscillator shell $N_{\rm shell}$, harmonic oscillator frequency $\hbar\omega$, and so on). The dependence of the numerical results on the parameters of the basis functions will be studied before the heavier nuclei are treated in future calculations.

(3) In calculating the numbers of transferred nucleons, we followed Washiyama's method proposed in the TDHF framework. It would be necessary to study the present results from the quantum mechanical viewpoint by making use of the number projection method [22].

(4) The present contribution shows that there is a dependence of the observables on the initial gauge angle. Nevertheless, the two fragments should initially respect the gauge angle symmetry and preserve the initial good number of particles in each fragment. It would be interesting for future applications to develop a self-consistent time-dependent mean-field theory that describes the evolution of a quasiparticle state projected on the good number of particles.

The transfer mechanism of nucleons in the collision processes of superfluid nuclei will be studied in a future analysis by combining the present method of solving the Gogny-TDHFB equations with the quantum mechanical method of number projection [22].

ACKNOWLEDGMENTS

The authors thank the members of the DFT meeting for exciting discussions. One of the authors (Y.H.) thanks Professor T. Nakatsukasa for discussions and comments. G.S. acknowledges the Japan Society for the Promotion of Science (Japan) for support through a JSPS postdoctoral fellowship for foreign researchers. This work was supported by Grant-in-Aid for JSPS Fellows No. 14F04769. This research work is partly supported by results of HPCI Systems Research Projects (Project IDs hp140010 and hp150081). Part of the numerical calculations were carried out on the SR16000 at YITP of Kyoto University. The numerical calculations were partly performed using COMA at the CCS of the University of Tsukuba.

[1] A. Bohr and B. R. Mottelson, *Nuclear Structure* (Benjamin, New York, 1975).
[2] P. Ring and P. Schuck, *The Nuclear Many-Body Problems* (Springer-Verlag, Berlin, 1980).
[3] R. A. Broglia and A. Winther, *Heavy Ion Reactions* (Westview Press, Boulder, 2004).
[4] G. Scamps, C. Simenel, and D. Lacroix, Phys. Rev. C **92**, 011602(R) (2015).
[5] A. Bulgac, P. Magierski, K. J. Roche, and I. Stetcu, Phys. Rev. Lett. **116**, 122504 (2016).
[6] P. Bonche, S. Koonin, and J. W. Negele, Phys. Rev. C **13**, 1226 (1976).
[7] J. W. Negele, Rev. Mod. Phys. **54**, 913 (1982).
[8] J. A. Maruhn, K. T. R. Davies, and M. R. Strayer, Phys. Rev. C **31**, 1289 (1985).
[9] A. S. Umar, M. R. Strayer, R. Y. Cusson, P. G. Reinhard, and D. A. Bromley, Phys. Rev. C **32**, 172 (1985).
[10] T. Nakatsukasa and K. Yabana, Phys. Rev. C **71**, 024301 (2005).
[11] A. S. Umar and V. E. Oberacker, Phys. Rev. C **74**, 021601(R) (2006).
[12] K. Washiyama and D. Lacroix, Phys. Rev. C **78**, 024610 (2008).
[13] A. S. Umar, V. E. Oberacker, J. A. Maruhn, and P. G. Reinhard, Phys. Rev. C **80**, 041601 (2009).
[14] D. J. Kedziora and C. Simenel, Phys. Rev. C **81**, 044613 (2010).
[15] C. Simenel and A. S. Umar, Phys. Rev. C **89**, 031601(R) (2014).
[16] Y. Hashimoto and K. Nodeki, arXiv:0707.3083.
[17] B. Avez, C. Simenel, and P. Chomaz, Phys. Rev. C **78**, 044318 (2008).
[18] S. Ebata, T. Nakatsukasa, T. Inakura, K. Yoshida, Y. Hashimoto, and K. Yabana, Phys. Rev. C **82**, 034306 (2010).
[19] I. Stetcu, A. Bulgac, P. Magierski, and K. J. Roche, Phys. Rev. C **84**, 051309 (2011).
[20] Y. Hashimoto, Eur. Phys. J. A **48**, 55 (2012).
[21] Y. Hashimoto, Phys. Rev. C **88**, 034307 (2013).
[22] G. Scamps and D. Lacroix, Phys. Rev. C **87**, 014605 (2013).
[23] B. D. Josephson, Phys. Lett. **1**, 251 (1962).
[24] B. D. Josephson, Rev. Mod. Phys. **36**, 216 (1964).
[25] V. I. Gol'danski and A. I. Larkin, Zh. Eksp. Teor. Fiz. **53**, 1032 (1967) [Sov. Phys. JETP **26**, 617 (1968)].
[26] K. Dietrich, Phys. Lett. B **32**, 428 (1970).
[27] K. Dietrich, Ann. Phys. (NY) **66**, 480 (1971).
[28] K. Dietrich, K. Hara, and F. Weller, Phys. Lett. B **35**, 201 (1971).
[29] M. Kleber and H. Schmidt, Z. Physik **245**, 68 (1971).
[30] R. A. Broglia, Ann. Phys. (NY) **80**, 60 (1973).
[31] C. Simenel, Phys. Rev. Lett. **105**, 192701 (2010).
[32] K. Sekizawa and K. Yabana, Phys. Rev. C **88**, 014614 (2013).
[33] K. Sekizawa and K. Yabana, Phys. Rev. C **90**, 064614 (2014).
[34] D. Baye and P. Heenen, J. Phys. A **19**, 2041 (1986).
[35] T. Matsuse, RIKEN Rev. **19**, 18 (1998).